Surface & Coatings Technology 206 (2011) 1744–1752

Contents lists available at SciVerse ScienceDirect

Surface & Coatings Technology

journal homepage: www.elsevier.com/locate/surfcoat

Mechanical and tribological properties evaluation of cathodic arc deposited CrN/ZrN multilayer coatings

Sung-Hsiu Huang [a], Siao-Fan Chen [b], Yu-Chu Kuo [b], Chaur-Jeng Wang [b], Jyh-Wei Lee [c,d,*], Yu-Chen Chan [e], Hsien-Wei Chen [e], Jenq-Gong Duh [e], Tsung-Eong Hsieh [a]

[a] Department of Materials Science and Engineering, National Chiao Tung University, Hsin-Chu, Taiwan
[b] Department of Mechanical Engineering, National Taiwan University of Science and Technology, Taipei, Taiwan
[c] Department of Materials Engineering, Ming Chi University of Technology, Taipei, Taiwan
[d] Center for Thin Films Technologies and Applications, Ming Chi University of Technology, Taipei, Taiwan
[e] Department of Materials Science and Engineering, National Tsing Hua University, Hsin-Chu, Taiwan

ARTICLE INFO

Available online 15 October 2011

Keywords:
Nanostructured multilayer coatings
Cathode arc evaporation
Bilayer period
CrN/ZrN

ABSTRACT

Five nanostructured CrN/ZrN multilayer coatings were deposited periodically by cathodic arc evaporation. The bilayer periods of the CrN/ZrN multilayer coatings were controlled in the range of 5 to 30 nm. The structures and bilayer period of the multilayer coatings were characterized by an X-ray diffractometer. The microstructures of thin films were examined by scanning electron microscopy (SEM) and transmission electron microscopy (TEM), respectively. Nanoindentation, scratch tests, Daimler–Benz Rockwell-C (HRC-DB) adhesion tests, microhardness and pin-on-disk wear tests were used to evaluate the hardness, adhesion, indentation toughness and tribological properties of thin films, respectively. It was found that the hardness and tribological properties were strongly influenced by the bilayer period of the CrN/ZrN multilayer coatings. An optimal combination of mechanical properties and excellent tribological behavior was found for a coating with a critical bilayer period of 30 nm.

1. Introduction

The surface engineering technology based on the plasma-assisted physical vapor deposition (PVD) has been developed for few decades [1] such as direct current (DC) magnetron sputtering, pulsed DC sputtering technology [2], or cathodic arc evaporation [3]. The cathodic arc evaporation (CAE) process is one of the most important developments in the PVD technology, which has been applied for tribological and cutting tools applications successfully due to the excellent mechanical properties of such coatings. Research work on TiN-based multilayered coatings like TiN/CrN [4] and TiN/ZrN [5,6] multilayered coatings has revealed that excellent mechanical properties were achieved due to the combination of suitable nanoscale multilayered features. For example, a longer cutting life was achieved for HSS saw blades coated with TiN/ZrN multilayers [5]. In addition, the hardness of TiN/ZrN multilayer coatings was enhanced as the bilayer period, Λ, increased to 15.54 nm [6]. After reaching the optimal hardness, the coatings showed a loss of hardness as the bilayer period decreased to 8 nm [6]. However, only limited reports are available on multilayered CrN/ZrN coatings with different thickness ratios, deposited either by DC [7–10] or by radio frequency (RF) [11] magnetron sputtering. Furthermore, anticorrosion properties of CAE deposited ZrN/CrN bilayer coatings were discussed [12]. No reports on CAE deposited CrN/ZrN multilayered coatings with equal thickness ratio of CrN to ZrN have been revealed. The dependence of the mechanical properties and toughness of CAE fabricated CrN/ZrN multilayer coatings on the bilayer periods has not yet been described. In this study, the CAE process was employed to fabricate CrN/ZrN multilayered coatings on titanium carbide (TiC) and Si substrates. TiC was selected due to its mechanical properties and is frequently applied as material for tool bits in cutting industry. Particularly, the thickness ratio of CrN to ZrN was designed to be 1:1 for each multilayer coating in this work. The influence of the bilayer period on the microstructure, mechanical, toughness and tribological properties is discussed. A wide variety of mechanical and tribological characterization techniques were adopted. The results are discussed in light of the microstructure of the films, illustrated by high quality SEM and TEM micrographs. The motivation of this work was to propose suitable bilayer periods for CrN/ZrN multilayer thin films with high hardness, good adhesion and tribological performance.

2. Experimental procedure

Five CrN/ZrN multilayered thin films with the same thickness ratios of CrN: ZrN layers = 1:1, and monolayer CrN and ZrN coatings were deposited on P-type (100) silicon wafers and TiC substrates by a cathodic arc evaporation system (KMARC, Kuen Min Tech. Co., Taiwan). Cr and Zr

* Corresponding author at: Department of Materials Engineering, Ming Chi University of Technology, Taipei, Taiwan. Tel.: +886 2 29089899x4437; fax: +886 2 29084091.

0257-8972/$ – see front matter © 2011 Elsevier B.V. All rights reserved.
doi:10.1016/j.surfcoat.2011.10.029

targets with 99.99 wt.% purity and 101.6 mm diameter were applied. The Zr and Cr targets were in opposite positions and the substrates were mounted on two sides of a rotating barrel between the two targets. Multilayered coatings were deposited by alternately rotating the substrates between the plasma of Cr and Zr targets. The target current values of Cr and Zr were adjusted to 70 A to achieve a fixed thickness ratio of CrN to ZrN around 1:1. Various values of the bilayer period Λ were achieved by controlling the substrate holder rotation speed in the plasma stream from the Cr or Zr target. The deposition chamber was pumped down to a base pressure of 1.0×10^{-2} Pa. All samples were cleaned by Ar ion bombardment for 15 min at 1.2 Pa in pure argon at a DC bias of −750 V. A pure CrZr interlayer around 60 nm thick was deposited as an adhesion layer. The CrN/ZrN multilayer films were deposited in an Ar and N_2 mixed plasma operated at a pressure of 0.86 Pa. A low heating temperature, 150 °C was used for all specimens during the deposition processes to avoid the deformation of substrates. The typical deposition conditions for each coating are listed in Table 1.

The chemical composition of the coatings was determined by a field emission electron probe microanalyzer (FE-EPMA, JXA-8500 F, JEOL, Japan) with an atomic number (Z), absorption (A) and fluorescence (F) corrected program [13]. Glancing angle X-ray diffraction (XRD-6000, Shimadzu, Japan) with an incidence angle of 2° and low-angle X-ray reflectivity (XRR) were utilized to study the crystal structure and the bilayer period (Λ) of each coating, respectively. The lateral grain size of the multilayered coatings was estimated by using the Scherrer formula via the integral width of a Bragg reflection [14]. The surface roughness of each thin film deposited on Silicon substrate was analyzed by atomic force microscopy (DI-3100, Bruker, USA) with a scan area of 5×5 μm. The surface and cross sectional morphologies of coatings on Si substrates were observed by field emission scanning electron microscopy (FE-SEM, JSM-6701F, JEOL, Japan) and transmission electron microscopy (TEM, JSM-2100, JEOL, Japan), respectively. The nanohardness and elastic modulus of thin films on Si substrates were measured by means of a nanoindenter (TI-900, TriboIndenter, Hysitron, USA) using a Berkovich 142.3° diamond probe at a maximum applied load of 5 mN. Ten indentations were made on the surface without macroparticle and pin hole defects for each coating. The maximum indentation depth was limited to around 50–60 nm, which was around the one-tenth of the film thickness. The loading and unloading rates of the nanoindentation were all 1000 μN/s. The holding time was 5 s. The hardness and elastic modulus of each indent were determined on the basis of the Oliver and Pharr method [15]. The elastic modulus, E, was expressed as follows

$$\frac{1}{E_r}=\frac{1-\nu^2}{E}+\frac{1-\nu_i^2}{E_i} \tag{1}$$

where E_r and ν are the reduced elastic modulus and Poisson's ratio, respectively, for the thin film under test, and E_i (1140 GPa) and ν_i (0.07) are the corresponding parameters of the diamond indenter. A micro Vickers hardness tester was used to further evaluate the indentation toughness, K, of coatings on Si substrates based on the following equation [16]:

$$K=\delta\left(\frac{P}{c^{3/2}}\right)\sqrt{\frac{E}{H}} \tag{2}$$

where P is the applied indentation load and δ is an indenter geometry constant, equal to 5 N and 0.016, respectively, for a Vickers diamond pyramid indenter. E, H and c are elastic modulus, hardness and radial crack length of the coating, respectively. The radial crack length was evaluated using a SEM. It should be noticed that the indentation toughness value, K, derived according to Eq. (2) is different from the fracture toughness, K_{IC}, obtained based on a clearly defined sample geometry and test condition.

A scratch test (Scratch Tester, J & L Tech. Co., Korea), up to a maximum load of 100 N, and the Daimler–Benz Rockwell-C (HRC-DB) adhesion test were adopted to explore the adhesion properties of thin films on TiC substrates. A pin-on-disk wear test method was used to investigate the wear resistance of coatings on Si substrates. A cemented tungsten carbide (WC-6 wt.% Co) ball, 5 mm in diameter was adopted as the stationary pin due to its high hardness. A normal load of 5 N was applied. The sliding speed was 27.2 mm/s with a wear track diameter of 8 mm. The test temperature was 20 °C, and the relative humidity was kept at 60%. The wear time was 30 min for each test. The wear rate of each coating was determined based on the following equation [17]:

$$W_R=\frac{t(3t^2+4b^2)2\pi r}{6bF_nS} \tag{3}$$

where t is the depth of the wear track determined using a surface profilometer, b is the width of the wear track, r is the radius of the wear track, F_n is the normal load and S is the sliding distance.

Table 1
Deposition parameters for monolayer CrN, ZrN and CrN/ZrN multilayered coatings.

Sample designation	CrN	ZrN	A1	A2	A3	A4	A5
Designed bilayer period (nm)	–		30	20	16	6	5
Holder rotation speed (Hz)	7.5		3.8	5	7.5	15	20
Zr target current (A)	0	70	70				
Cr target current (A)	70	0	70				
Base pressure (Pa)	1.0×10^{-2}						
Working pressure (Pa)	8.6×10^{-1}						
Substrate temperature (°C)	150						
Ar:N_2 gas ratio	1:7						
Total gas flows (sccm)	80						
Substrate bias (V)	−100						
Sputtering time (min)	24		26				

3. Results and discussion

3.1. Composition and phase characterization of CrN/ZrN multilayers

According to the FE-EPMA analysis, it was observed that similar chemical compositions were obtained for each coating as listed in Table 2. It is found that the ZrN is an under-stoichiometric ZrN_{1-y} and CrN is an over-stoichiometric CrN_{1+x}. The mean value of the chemical composition for the CrN/ZrN multilayered thin films were 31.9% Cr-24.7% Zr-43.2% N-0.2% O (in at.%). However, the EPMA analysis of multilayer coatings is probably a rough estimation. A depth sensing analyses, such as the Auger electron spectrometer should be adopted in the future to study the periodic change of Cr, Zr and N contents from CrN_{1+x} to ZrN_{1-y} layers. The glancing angle XRD patterns of monolayer CrN, ZrN and CrN/ZrN multilayer coatings deposited with different bilayer periods are shown in Fig. 1. Although the CrN is over-stoichiometric in N ($CrN_{1\pm x}$), the (111), (200), (220) and (311) reflections of the single layer CrN coating were observed. No β-Cr_2N phase is found due to a rather high N_2/Ar ratio during deposition process. On the other hand, the (111), (200), (220) and (311) reflections of the monolayer ZrN also can be observed, even though ZrN is sub-stoichiometric in N (ZrN_{1-y}). In addition, the XRD peaks of the Si substrate were also observed due to a high X-ray incidence angle, 2°, used to penetrate the coating.

For the CrN/ZrN multilayer coatings, some of the ZrN and CrN characteristic reflections can be observed for each coating. However, as compared with the monolayer ones, different XRD reflection intensities are observed for multilayered coatings. The diffraction peak of CrN (200) vanishes whereas the reflections along CrN (111) and ZrN (111) planes are formed in the multilayered thin films. A similar result was also explored for CrN/ZrN multilayer coatings by Zhang et

Table 2
Characteristics of the coatings: average coating thickness, surface roughness, grain size and chemical compositions.

Sample designation		CrN	ZrN	A1	A2	A3	A4	A5
Designed bilayer period (nm)		–		30	20	16	6	5
Average coating thickness (nm)		400	420	511	571	677	508	527
Surface roughness (nm)		1.1 ± 0.43	0.24 ± 0.02	0.94 ± 0.50	2.61 ± 1.03	2.52 ± 2.23	1.13 ± 0.07	1.14 ± 0.54
Average grain size (nm)		10.74	6.30	4.57	4.19	4.69	2.90	3.72
Chemical composition (at.%)	Cr	44.5	–	32.8	34.1	27.8	31.3	33.4
	Zr	–	60.0	22.3	21.9	30.3	26.3	22.9
	N	53.1	36.4	44.8	43.8	41.3	42.3	43.6
	O	2.4	3.6	0.1	0.2	0.6	0.1	0.1

al. [10]. It was suggested that this (111) crystalline structure would be associated with the internal stress relieving of the thin films [4,10].

When the bilayer period decreases, the positions of the CrN diffraction peaks shift to a lower diffraction angle, whereas the positions of the ZrN diffraction peaks shift toward a higher diffraction angle. On the other hand, the peak intensities of samples A4 and A5 decrease as the bilayer period decreases down to 6 and 5 nm. Apparently, a higher degree of crystallization of the multilayer thin films at higher bilayer periods is observed. It is suggested that the coherency breaking occurs in all CrN/ZrN multilayer coatings. The crystallinity gets lost at low bilayer periods and increases with the thickness of CrN and ZrN layers. The calculated average grain size of each coating is listed in Table 2. A larger grain size around 4 nm is observed for multilayer coatings with a bilayer period larger than 6 nm. On the other hand, a smaller grain size around 3 nm can be found for the A4 and A5 coatings with smaller bilayer periods.

Fig. 2 depicts the X-ray reflectivity patterns of CrN/ZrN multilayers with calculated bilayer periods. The bilayer period was calculated based on the modified form of Bragg's law [18]:

$$\sin 2\theta = (m\lambda/2\Lambda)^2 + 2\delta, \quad (4)$$

where m is the order of the reflection, λ is the X-ray wavelength, Λ is the bilayer period and δ is the real part of the average refractive index of X-rays within the film [18]. According to Fig. 2, the calculated thickness of the bilayer period is slightly smaller than the designed value for each coating. A maximum deviation from its designed values around 11.9% is found for the A3 coating.

3.2. Microstructure characterization of CrN/ZrN multilayers

Fig. 3(a) to (d) illustrates the SEM surface morphologies of monolayer CrN, ZrN, A1 and A3 CrN/ZrN multilayer coatings, respectively. In general, macroparticles and pin holes can be found for each coating. A rather smooth surface can be found for the metal-rich ZrN thin film as shown in Fig. 3(b), which is possibly due to a new Zr metal target used during deposition process. However, many macroparticles and deep pin holes are observed on the surface of the A3 coating. It is suggested that the arc discharge on the target surface would produce metallic macroparticles and then splattered to the coating surface during deposition process [3]. The spalling of macroparticles thus produced the so-called pin holes on the thin film surface. The surface roughness of each coating was further evaluated by an AFM. A typical fine granular structure with macroparticles and pin holes was observed on the surface of each coating. The average surface roughness, Ra, for each thin film is listed in Table 2. In general, the value of the bilayer period shows no direct influence on the surface roughness of the multilayer coatings.

Fig. 4(a), (b), and (c) illustrate the cross-sectional back scattered electron images (BEI) of the A1, A3, and A4 coatings, respectively. A dense and compact multilayer structure with columnar grains was observed for each coating. A pure CrZr interlayer can be seen between the coating and Si substrate. The thickness values of the multilayer coatings are listed in Table 2. Thickness values ranging from 508 to 677 nm are observed. However, in case of the A5 coating with a

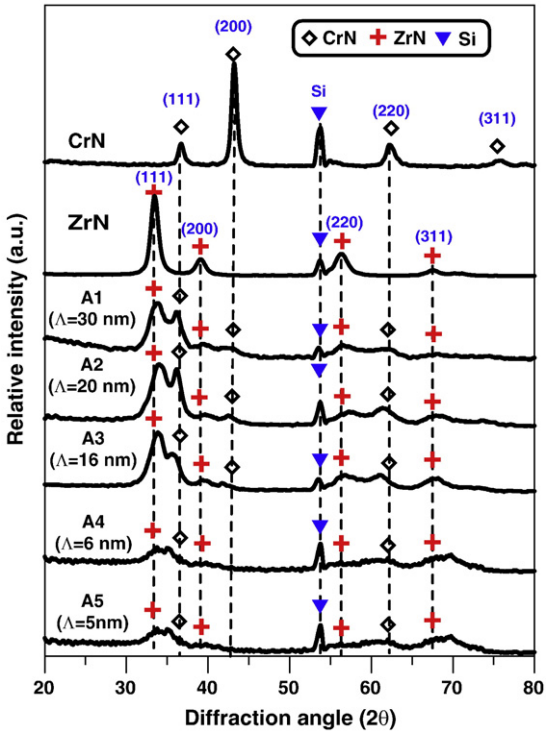

Fig. 1. Glancing angle X-ray diffraction patterns of the CrN, ZrN and CrN/ZrN multilayered coatings with different bilayer periods on Si substrates.

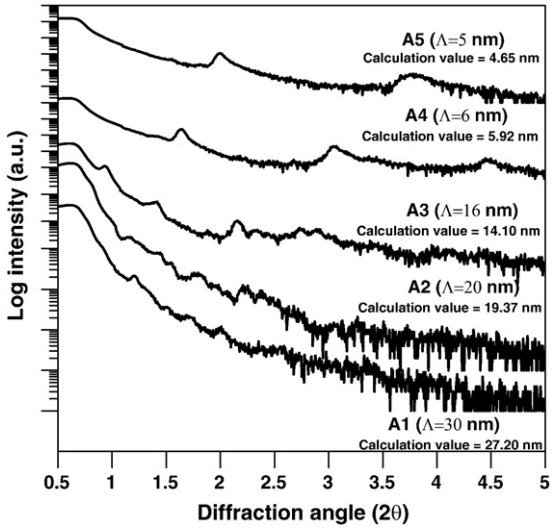

Fig. 2. X-ray reflectivity patterns of the CrN/ZrN multilayered thin films on Si substrates.

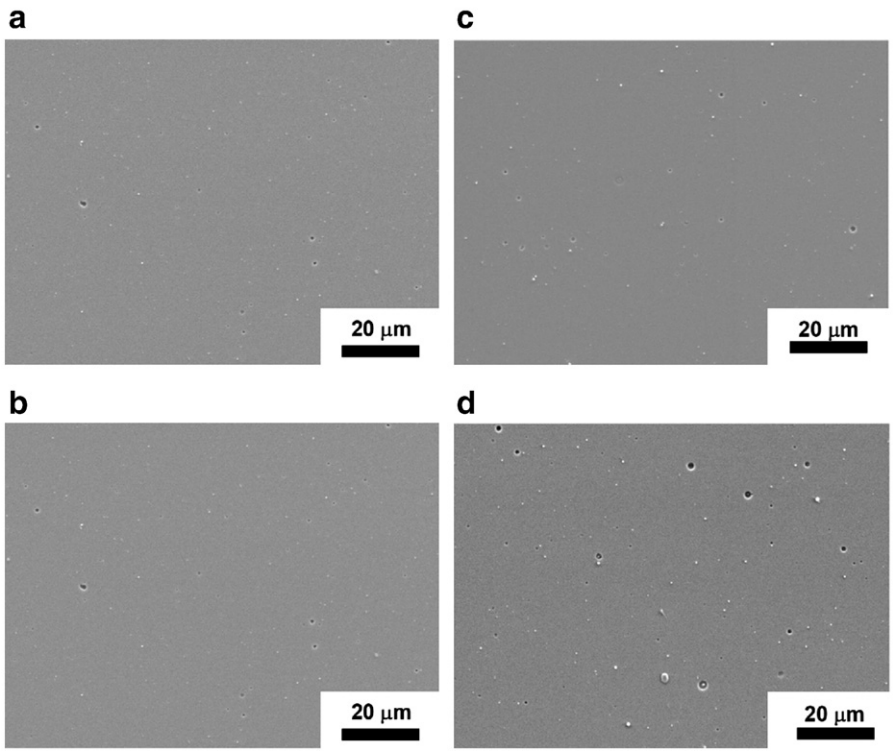

Fig. 3. SEM surface morphologies of the (a)CrN, (b)ZrN, (c)A1 and (d) A3 thin films on Si substrates.

bilayer period of 5 nm, the multilayered nanostructure is difficult to recognize due to the resolution limits of the FE-SEM. The TEM technique was further adopted to explore the detailed microstructure of the multilayer coating A5 with $\Lambda = 5$ nm.

The low magnification cross-sectional TEM micrograph of the A5 coating is depicted in Fig. 5(a). The laminated structure along with long columnar grains (marked with arrows) around several tens nm in width are observed throughout the whole multilayer coating. The cross-sectional TEM micrograph of the A5 coatings at higher magnification is shown in Fig. 5(b). Clear laminated and columnar structures can be observed. The alternating gray and dark color regions represent the CrN and ZrN layers (indicated by arrows), respectively. The average thickness values of the CrN and ZrN layers are 2.50 nm and 2.20 nm respectively, which is very close to the design value of 5 nm of Λ. According to the cross-sectional SEM and TEM micrographs shown in Figs. 4, 5 and the XRR data revealed in Fig. 2, the nanolayered structures with sequentially alternating CrN and ZrN layers are confirmed. It is also concluded that the bilayer period thickness deviates from the design value less than 11.9%. It should be noticed that the nanolayered structure of CrN/ZrN coatings is not the superlattice type due to the large mismatch between CrN and ZrN lattices about 10% in this work.

3.3. Mechanical and tribological properties of CrN/ZrN multilayered thin films

The hardness and elastic modules of the CrN/ZrN multilayered coatings as a function of bilayer period are shown in Fig. 6. The hardness and elastic modulus values of the monolayer CrN and ZrN coatings are also inserted. The average hardness and elastic modules of CrN and ZrN are 20.3, 228 GPa and 21.9, 267 GPa, respectively. It is observed that the hardness is low, around 22–23 GPa when $\Lambda = 5$–6 nm and reaches a maximum value, 25.2 GPa at $\Lambda = 16$ nm and, followed by a leveling off when the bilayer period increases to values higher than 16 nm. A maximum hardness reaches to 25.2 GPa was found for the A3 coating with 16 nm bilayer period, whereas a minimum hardness of 22.2 GPa was found for the A4 coating with $\Lambda = 6$ nm. A similar tendency of the hardness versus the Λ value was reported for TiN/ZrN multilayer coatings [4]. It should be pointed out that the hardness and elastic modules of each CrN/ZrN multilayered coating are still higher than that of single layer CrN and ZrN thin films. A similar tendency was also revealed for CrN/ZrN multilayer coatings [10]. The hardness kept a constant when the bilayer period ranged from 11.7 to 66.7 nm [10]. It can be concluded that the bilayer period thickness plays a critical key role for the mechanical properties of CrN/ZrN multilayer coatings.

The plastic deformation resistance values, H^3/Er^2 of the CrN/ZrN multilayered coatings, versus the bilayer periods are illustrated in Fig. 6. Results of monolayer CrN and ZrN coatings are also inserted. It should be pointed out that a large data scattering of the elastic modules is observed for multilayer coatings at $\Lambda = 16$–30 nm, which should show certain influences on the statistics of the H^3/Er^2 values. Nevertheless, the plastic deformation resistance value of each multilayered coating is higher than that of single layer CrN and ZrN thin films. The maximum plastic deformation resistance, 0.30 GPa was reached when the bilayer period was 16 nm, which also exhibits the maximum values of hardness and elastic modules. However, a different trend is performed in the relationship between the plastic deformation resistance and the bilayer period. A minimum value of 0.22 GPa is obtained for the A2 coating ($\Lambda = 20$ nm).

In this work, a moderate enhancement of the hardness of the CrN/ZrN multilayered coatings as compared with single layer CrN and ZrN coatings was clearly observed. It is well known that the hardness increasing to a maximum value and then decreasing as the bilayer period increases is a typical phenomenon observed in multilayered coatings [19]. In such multilayer systems, the hardness enhancement mechanism can be explained by the Koehler theory [20] or by the alternating-stress strengthening theory [21], which is based on the blocking of dislocations at interfaces.

In this study, the hardness enhancement of the CrN/ZrN coatings compared with single layer CrN and ZrN coatings ($H_{CrN} = 20.3$ GPa,

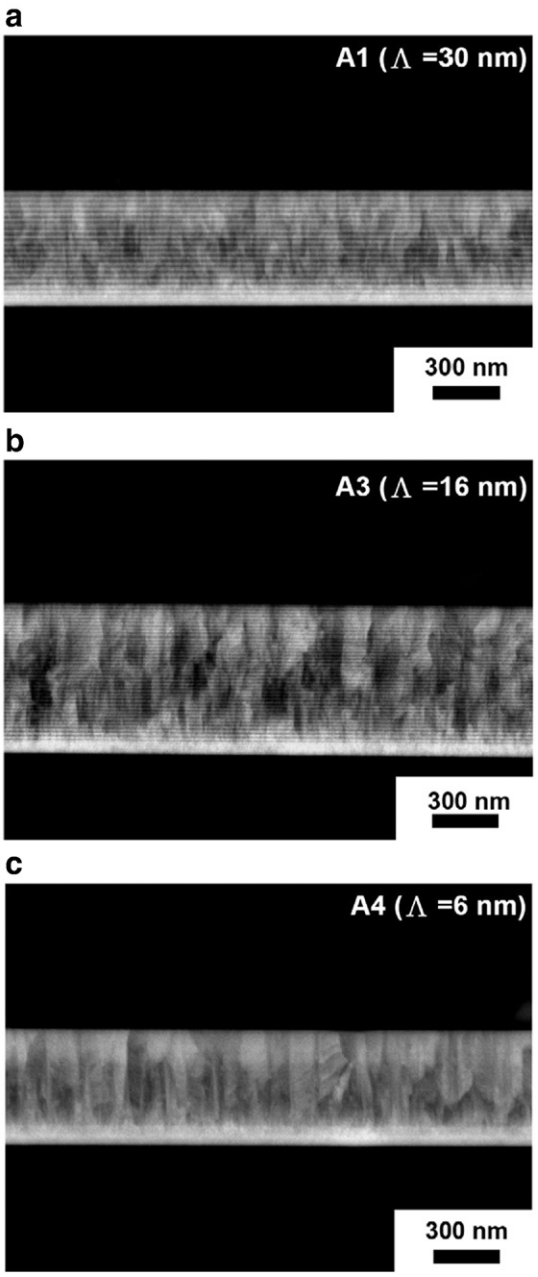

Fig. 4. The cross-sectional SEM morphologies of the (a) A1, (b) A3 and (c) A4 multilayered coatings on Si substrates.

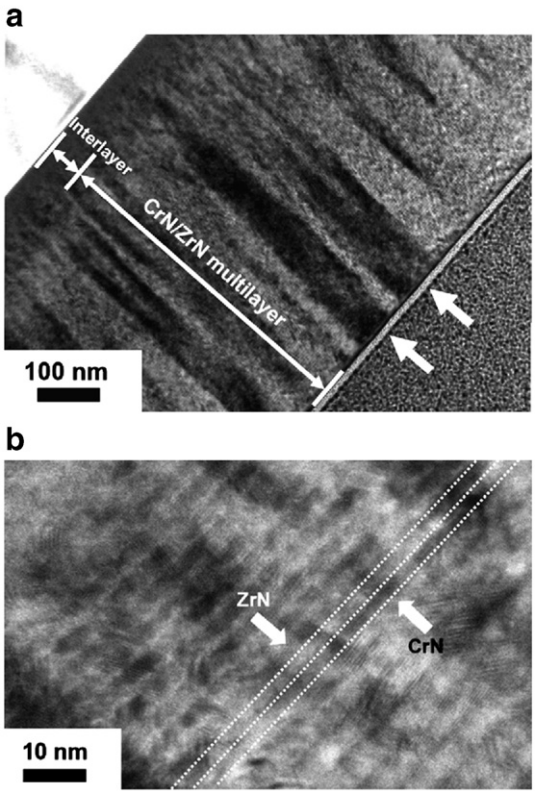

Fig. 5. The cross-sectional TEM micrographs of the A5 coating on Si substrate at (a) lower and (b) higher magnifications.

$H_{ZrN} = 22$ GPa) may be calculated according to the Koehler theory [20] in Eq. (5):

$$\Delta H_{max} = \frac{3RG_A \sin\theta}{8\pi m} \quad (5)$$

where $R = (G_B - G_A)/(G_B + G_A)$, G_A and G_B are shear module of the two layers, respectively, and $G_B > G_A$, The Taylor factor, m, is 0.3 for transition metal nitride, such as CrN and ZrN, whereas θ is the smallest angle between the interface and the glide plane of the lower modulus layer. And $G = E/2(1+\nu)$ (E is the elastic modulus and ν is the Poisson's ratio). Using the data obtained from the single layer films, $E_{CrN} = 228$ GPa and $E_{ZrN} = 267$ GPa, in this work, the Poisson's ratios are 0.2 for both CrN and ZrN, and θ is 45° for the multilayer coating, the shear modulus values of the CrN and ZrN can be calculated to 95 GPa and 111 GPa, respectively. Based on Eq. (5), a hardness enhancement, ΔH of around 2 GPa as compared with that of monolayer CrN can be achieved. However, a higher hardness enhancement of 4.9 GPa can be found for the A3 coating with the maximum hardness. Mendibide et al. [4] discussed the mechanical property enhancement in TiN/ZrN multilayers by the fluctuating stress field generated at each TiN/ZrN interface due to their similar lattice parameters. However, this model may not be adopted for CrN/ZrN films due to the large mismatch between the CrN and ZrN lattices, which are 0.414 nm and 0.457 nm, respectively. Although the residual stress is not determined, it is suggested that the alternating-stress strengthening mechanism [21] has possibly strong influence on the hardness enhancement of CrN/ZrN coatings in this work. In addition, the significant deviation in stoichiometry between CrN_{1+x} and ZrN_{1-y} will contribute to periodical stress modifications at interfaces.

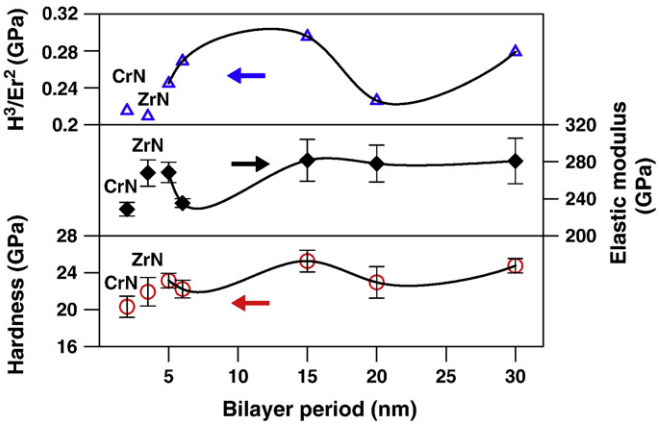

Fig. 6. The relationships between the hardness, elastic modulus, plastic deformation resistance and bilayer periods for the CrN/ZrN multilayered coatings on Si substrates.

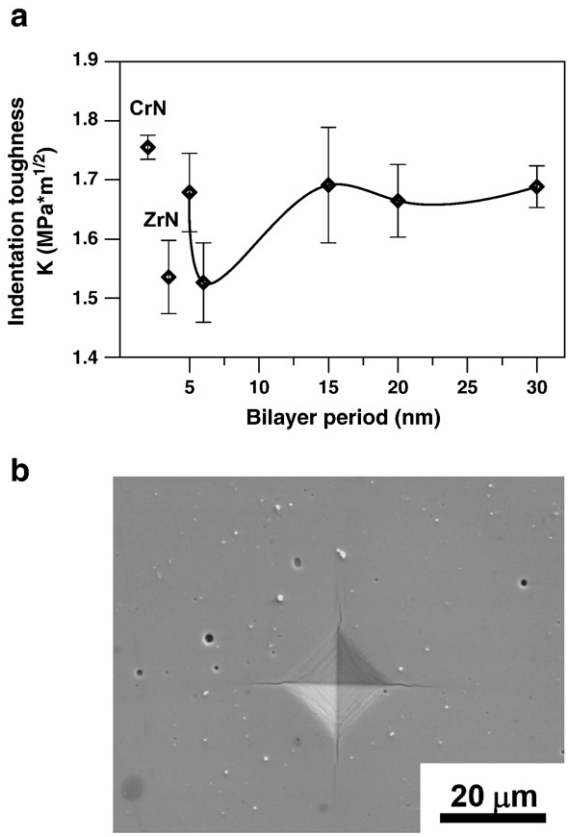

Fig. 7. (a)The indentation toughness as a function of bilayer period for the CrN/ZrN multilayered coatings on Si substrates and (b) the surface morphology of radial cracks for the A3 coating.

The toughness measurement of thin films is difficult and no standard procedure was established yet [22]. Among several toughness measurement methods, such as the bending, buckling, scratching, indentation and tensile test, the indentation method is widely used because of its simplicity [22]. The indentation toughness, K, of the CrN/ZrN multilayered coatings versus the bilayer period is shown in Fig. 7(a). The surface morphology of radial cracks for the A3 coating is shown in Fig. 7(b). The indentation toughness values of the monolayer CrN and ZrN coatings are around 2.06 MPa$\sqrt{m}$ and 1.83 MPa$\sqrt{m}$, respectively. In literature, CrN is characterized for its good toughness [23,24]. Similar high toughness values were also reported for CrSiN coatings in a previous work [25]. In comparison, the values of indentation toughness for multilayered coatings are between those of the CrN and ZrN coatings. However, a minimum values, 1.88 MPa$\sqrt{m}$, can be found for the A4 coating with $\Lambda = 6$ nm. A similar tendency is observed as compared with the mechanical properties of multilayered coatings illustrated in Fig. 6. The indentation toughness values of multilayered coatings are kept about the same when the bilayer period decreases from 20 nm to 16 nm and then decreases at $\Lambda = 6$ nm. Finally, the K value increases when the bilayer period is approximately 5 nm. A higher indentation toughness, 2.15 MPa$\sqrt{m}$, is obtained for the A1 coating ($\Lambda = 30$ nm) with a high hardness and plastic deformation, which is possibly attributed to the thick CrN layer. The reason for the rather low indentation toughness for the A4 coating is possibly attributed to its low elastic modulus. It is suggested that through a suitable control of the bilayer period and the stoichiometry in composition, a multilayered coating can act as a crack inhibitor to achieve high hardness, adequate fracture resistance and high toughness values simultaneously [26–29]. In multilayered coatings, the crack propagation toward the substrate can be retarded by the interfaces, whereas the cracks propagating straight downward to the substrate is often found in single layer coatings. Due to the deflection of cracking at every layer interface, reduced stress intensities at the crack tip are thus observed. Consequently, more energy is required for the cracking to propagate again at the interface and this leads to a tougher coating [28]. Compared with the mechanical properties results depicted in Figs. 6 and 7, it is confirmed that the bilayer period of the CrN/ZrN multilayered coatings should be prepared in a moderate range to achieve high levels of toughness and an adequate hardness, such as the A3 and A1 coatings with $\Lambda = 16$ nm and 30 nm, respectively. It should be noticed that the lower hardness of the A3 coating, 12 GPa, was achieved by the Vickers micro hardness test due to its higher loading force and deeper indentation depth, around 2.7 μm, which was mainly the hardness of the Si substrate.

According to the HRC-DB test [30], the adhesion level from HF1 to HF4 exhibits sufficient adhesion quality, whereas HF5 and HF6 represent insufficient adhesion. In this work, the HF value of each coating is HF1, except of the A3 coating, which is HF3. Nevertheless, all coatings exhibit excellent adhesion quality, which is in good agreement with previous work [31]. No spallation or chipping of coatings is found. Only some radial cracks adjacent to the impact crater can be observed.

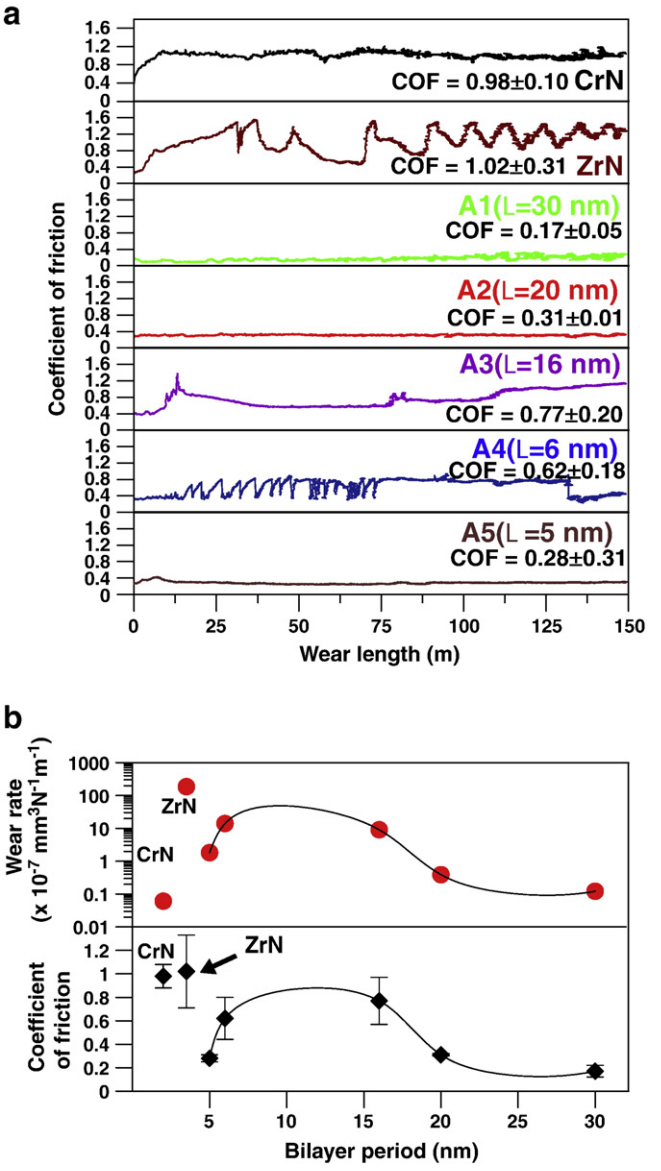

Fig. 8. (a) The coefficient of friction (COF) versus the wear length, (b) the COF and wear rate with respect to the bilayer period for the CrN, ZrN and multilayered coatings on Si substrates against a WC–Co ball.

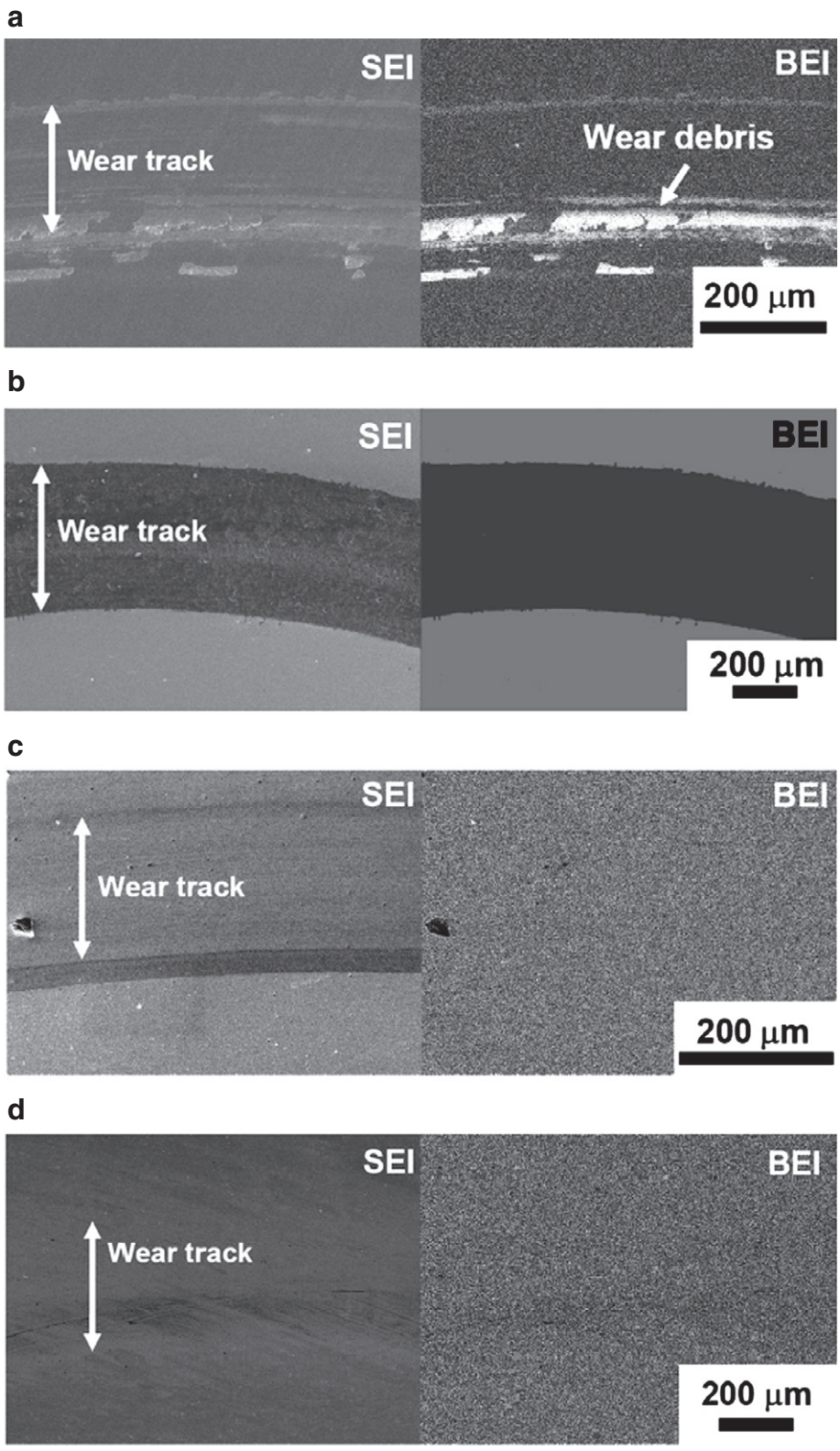

Fig. 9. The SEI and BEI micrographs of wear scar morphologies for the (a) CrN, (b) ZrN, (c) A1, (d) A2, (e) A3, (f) A4 and (g) A5 coatings after the pin-on-disk wear test.

The critical load obtained from the scratch test can be used to estimate the adhesion of the coatings. The critical loads of all monolayer and multilayered coatings are higher than 100 N, indicating excellent adhesion achieved in this study. No cracking or delamination of coatings inside or adjacent to the scratch track is observed.

Fig. 8(a) illustrates the coefficient of friction (COF), measured in pin-on-disk tests, versus the wear length of all thin films. The average COF values and wear rates versus bilayer period are also displayed in Fig. 8(b). The corresponding results of monolayer CrN and ZrN are also marked. The average COF values of the single layer CrN and ZrN

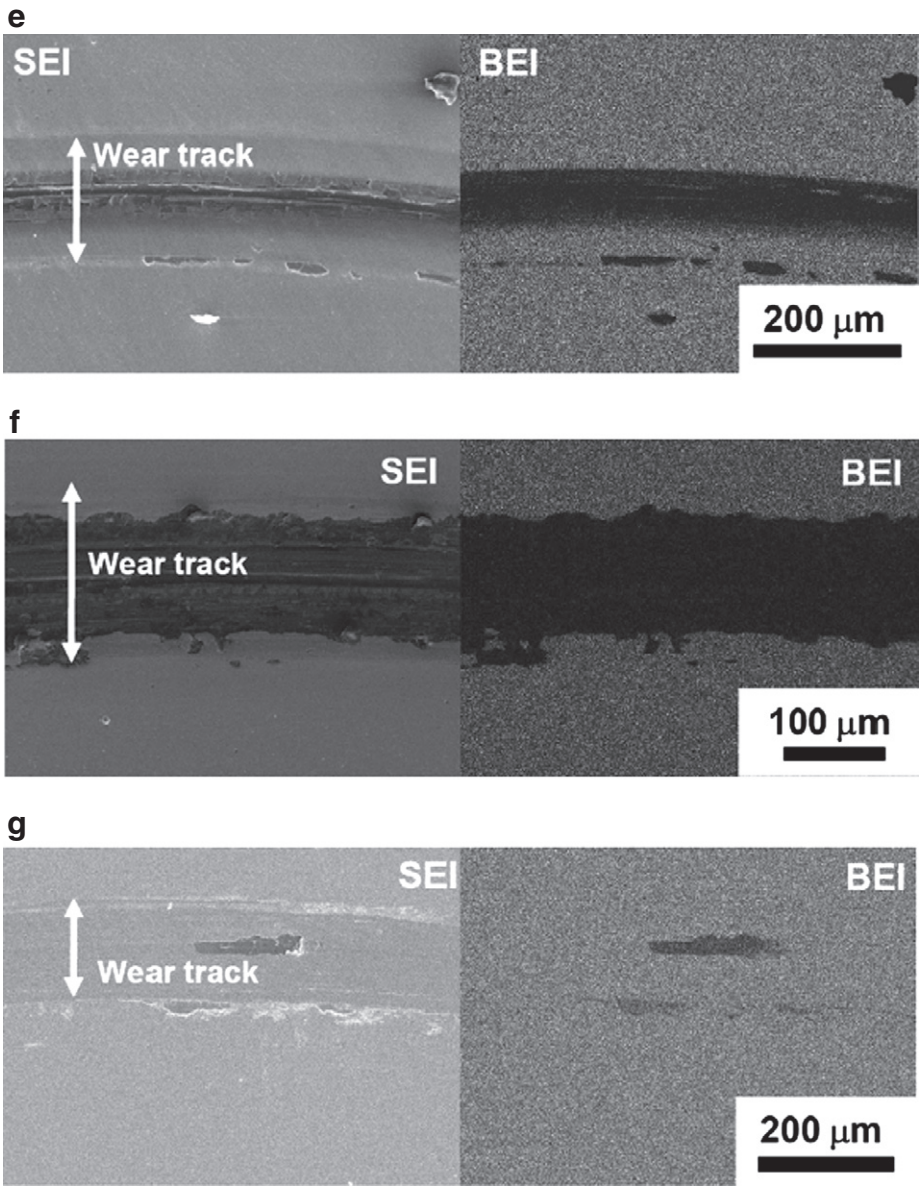

Fig. 9 (*continued*).

are around 1.0, respectively. In contrast, the COF values of CrN/ZrN multilayered coatings were lower than those of the single layer coatings. A minimum COF around 0.17 ± 0.05 was found for the A1 coating with $\Lambda = 30$ nm. A rather low COF value was also obtained for the A5 coating when $\Lambda = 5$ nm. For multilayered coatings, it is obvious that the COF values are affected by the bilayer period and show a similar tendency as compared with the wear rate. The COF value increases gradually when the bilayer period decreases from 30 nm to 16 nm and then decreases as the bilayer period is around 5–6 nm.

The CrN film shows significant lower wear rate as compared with that of the ZrN monolayer. However, a higher wear rate is obtained for each multilayered coating as compared with the CrN monolayer. For the coatings with $\Lambda > 5$ nm, the wear rate decreases with increasing bilayer period in this work. Similarly, Zhang et al. [8] found that the wear resistance of CrSiN/ZrN multilayered coatings was enhanced by increasing the bilayer period thickness. It is suggested that the better wear rate of multilayered coatings with larger Λ value is possibly attributed to the thicker layer of the CrN, which exhibits high indentation toughness and good wear resistance to compensate for the poor wear performance of the ZrN layer.

The secondary electron images (SEI) and backscattered electron images (BEI) of wear scar morphologies for the CrN, ZrN monolayers and CrN/ZrN multilayered coatings are shown in Fig. 9(a)–(g), respectively. A narrow wear track, around 200 μm wide, is found for the monolayer CrN coating. No crack is observed in the wear track. As compared with the SEI and BEI micrographs shown in Fig. 9(a), some white debris as indicated by an arrow are found inside and adjacent to the wear track, which are tungsten rich oxide wear debris identified by EDS. The entrapment of cemented tungsten carbide (WC/Co) ball debris into the hard coatings has been revealed in the wear test of CrN coatings in previous work [31,32]. On the other side, the ZrN coating is totally worn through and the substrate is thus exposed as shown in Fig. 9(b), which implies a poor wear resistance of the ZrN thin film. The zigzag shape of COF for the ZrN coating shown in Fig. 8(a) also indicates its poor wear behavior. It is suggested that the poor anti-wear performance of the ZrN monolayer is attributed to the lowest plastic deformation resistance and the lower indentation toughness value shown in Figs. 6 and 7(a) and is also possibly related to the nitrogen deficiency of coating.

In contrast, the wear scar morphologies of the A1 coating are shown in Fig. 9(c). A smooth wear track was found in this case. No

cracking or delamination was observed adjacent to the wear track. A similar result is also found for the A2 coating illustrated in Fig. 9(d). A smooth wear scar and partial delamination of the coating are observed for the A5 coating depicted in Fig. 9(g). On the other hand, severe spallation in the wear track is found for the A4 coating shown in Fig. 9(f). The zigzag shape of COF for the A4 coating shown in Fig. 8(a) also indicates its poor wear behavior. More spallation regions are also observed for the A3 coating depicted in Fig. 9(e), which exhibits a higher wear rate and a high COF value. It has been reported [33,34] that the multilayer structure design, including the type of films, the number and thickness of interlayers can be adjusted to improve the mechanical properties and toughness of thin films. In this work, the layer by layer wear mechanism is also valid for the CrN/ZrN multilayered coating system [10]. The tougher surface CrN layer begins to wear until fatigue cracks occur, which can propagate and reach the CrN/ZrN interface. Therefore, this CrN layer is delaminated and the underlying ZrN layer is exposed to the wear loading. Furthermore, after a ZrN layer was worn through, a fresh tougher CrN surface starts to wear and the process repeats again. It is important to point out that the relative poor mechanical properties were found for the A4 coating. The exact reason still needs further investigation. However, the lowest thickness and the statistical effect of the CrN/ZrN multilayer structure revealed by XRD in Fig. 1 may be possible reasons for its poor mechanical properties.

4. Conclusion

Five CrN/ZrN multilayered thin films with different bilayer periods ranging from 5 to 30 nm were prepared by a cathodic arc evaporation process in this study. The CrN (111) and ZrN (111) crystal structures were found for the multilayered coating. Excellent adhesion properties were observed for each coating. It is found that the wear resistance in pin-on-disk tests was enhanced by increasing the bilayer period thickness. The maximum hardness, elastic modules and plastic deformation resistance values around 25.2 GPa, 282 GPa and 0.3 GPa, were obtained, respectively, for the A3 coating with 16 nm bilayer period. The highest indentation toughness and the lowest COF of 2.13 MPa $\sqrt{m}$ and 0.17 were achieved, respectively, for the coating with 30 nm bilayer period. It was concluded that a combination of excellent mechanical and adhesion properties, high plastic deformation resistance and good tribological performance has been achieved for the CrN/ZrN multilayered coating at $\Lambda = 30$ nm in this work.

Acknowledgment

The authors gratefully acknowledge the financial support of the National Science Council, Taiwan through contract no. NSC100-2622-E-131-001-CC2. The constructive comments by reviewers and editor to improve the quality of the manuscript are also highly appreciated.

References

[1] A. Matthews, J. Vac. Sci. Technol., A 21 (2003) S224.
[2] P.J. Kelly, R.D. Arnell, J. Vac. Sci. Technol., A 17 (1999) 945.
[3] R.L. Boxman, S. Goldsmith, Surf. Coat. Technol. 52 (1992) 39.
[4] C. Mendibide, P. Steyer, J. Fontaine, P. Goudeau, Surf. Coat. Technol. 201 (2006) 4119.
[5] S. Ulrich, C. Ziebert, M. Stuber, E. Nold, H. Holleck, M. Goken, E. Schweitzer, P. Schloßmacher, Surf. Coat. Technol. 188 (2004) 331.
[6] X.M. Xu, J. Wang, J. An, Y. Zhao, Q.Y. Zhang, Surf. Coat. Technol. 201 (2007) 5582.
[7] J.J. Zhang, M.X. Wang, J. Yang, Q.X. Liu, D.J. Li, Surf. Coat. Technol. 201 (2007) 5186.
[8] Z.G. Zhang, O. Rapaud, N. Allain, D. Mercs, M. Baraket, C. Dong, C. Coddet, Adv. Eng. Mater. 11 (2009) 667.
[9] D.J. Li, F. Lin, M.X. Wang, J.J. Zhang, Q.X. Liu, Thin Solid Films 506 (2006) 202.
[10] Z.G. Zhang, O. Rapaud, N. Allain, D. Mercs, M. Baraket, C. Dong, C. Coddet, Appl. Surf. Sci. 255 (2009) 4020.
[11] N.A. de Sánchez, H.E. Jaramillo, Z. Vivas, W. Aperador, C. Amaya, J.C. Caicedo, Adv. Mater. Res. 38 (2008) 63.
[12] J. Barranco, F. Barreras, A. Lozano, A.M. Lopez, V. Roda, J. Martin, M. Maza, G.G. Fuentes, E. Almandoz, Int. J. Hydrogen Energ. 35 (2010) 11489.
[13] J.I. Goldstein, D. Newbury, D. Joy, C. Lyman, P. Echlin, E. Lifshin, L. Sawyer, J. Michael, Scanning Electron Microscopy and X-ray Microanalysis, Plenum Press, 2003, p. 404.
[14] B.D. Gullity, S.R. Stock, Element of X-ray Diffraction, Prentice Hall, NJ, 2001, p. 170.
[15] M.C. Oliver, G.M. Pharr, J. Mater. Res. 7 (4) (1992) 1564.
[16] B.R. Lawn, A.G. Evans, D.B. Marshall, J. Am. Ceram. Soc. 63 (1980) 574.
[17] S. Ma, J. Procházka, P. Karvánková, Q. Ma, X. Niu, X. Wang, D. Ma, K. Xu, S. Veprek, Surf. Coat. Technol. 194 (2005) 143.
[18] P.C. Yashar, W.D. Sproul, Vaccum 55 (1999) 179.
[19] U. Helmersson, S. Todorova, S.A. Barnett, J.E. Sundgren, L.C. Markert, J.E. Greene, J. Appl. Phys. 62 (1987) 481.
[20] J.S. Koehler, Phys. Rev. B 2 (1970) 547.
[21] M. Kato, T. Mori, L.H. Schwartz, Acta Metall. 28 (1980) 285.
[22] S. Zhang, D. Sun, Y. Fu, H. Du, Surf. Coat. Technol. 198 (2005) 74.
[23] M. Nordin, M. Larsson, Surf. Coat. Technol. 116–119 (1999) 108.
[24] Z.G. Zhang, O. Rapaud, N. Allain, M. Baraket, C. Dong, C. Coddet, J. Vac. Sci. Technol., A 27 (2009) 672.
[25] M.K. Wu, J.W. Lee, Y.C. Chan, H.W. Chen, J.G. Duh, Surf. Coat. Technol. (2011), doi:10.1016/j.surfcoat.2011.07.045.
[26] H. Holleck, V. Schier, Surf. Coat. Technol. 76 (1995) 328.
[27] S.J. Bull, A.M. Jones, Surf. Coat. Technol. 78 (1996) 173.
[28] P. Panjan, M. Čekada, B. Navinšek, Surf. Coat. Technol. 174 (2003) 55.
[29] M. Stueber, H. Holleck, H. Leiste, K. Seemann, S. Ulrich, C. Ziebert, J. Alloys Compd. 483 (2009) 321.
[30] H. Jehn, G. Reiners, N. Siegel (Eds.), DIN Fachbericht 39, Characterisierung Dunner Schichten, Beuth Verlag, Berlin, 1993, p. 213.
[31] J.W. Lee, J.G. Duh, J.H. Wang, Surf. Coat. Technol. 168 (2003) 223.
[32] J.W. Lee, Y.C. Kuo, C.J. Wang, L.C. Chang, K.T. Liu, Surf. Coat. Technol. 203 (2008) 721.
[33] M. Nordin, M. Larsson, S. Hogmark, Wear 232 (1999) 221.
[34] S. Zhang, D. Sun, Y. Fu, H. Du, Surf. Coat. Technol. 198 (2005) 2.